Fabrication, structure and photoluminescence properties of Eu^{3+}-activated red-emitting $Ba_2Gd_2Si_4O_{13}$ phosphors for solid-state lighting*

LÜ Tian-shuai (吕天帅)[1], **XU Xu-hui** (徐旭辉)[1], **WANG Da-jian** (王达健)[2], **SUN Liang** (孙亮)[2], **and QIU Jian-bei** (邱建备)[1]**

1. College of Materials Science and Engineering, Kunming University of Science and Technology, Kunming 650093, China

2. School of Materials Science and Engineering, Tianjin University of Technology, Tianjin 300384, China

(Received 24 October 2013)

Eu^{3+}-activated red-emitting $Ba_2Gd_2Si_4O_{13}$ phosphors are prepared via microwave (MW) synthesis and solid-state (SS) method. The structural and luminescent properties of phosphors are investigated by X-ray diffraction (XRD), photoluminescence (PL) spectra and scanning electron microscopy (SEM). Upon 393 nm excitation, compared with the sample sintered by SS method, luminescence enhancement is observed in the sample synthesized by MW method. The mechanism of MW synthesis process is discussed in detail. Results indicate that the PL enhancement is probably related to the concave-convex phosphor surfaces and uniform grains, which may reinforce scattering of excitation light. Our research may further promote the understanding of MW synthesis and extend the application of Eu^{3+}-activated $Ba_2Gd_2Si_4O_{13}$ in white light-emitting diodes.

Document code: A **Article ID:** 1673-1905(2014)02-0106-5

DOI 10.1007/s11801-014-3210-z

White light-emitting-diodes (WLEDs) have attracted much attention because of their technical advantages and various potential applications in residential lighting and display field[1-4]. The present commercial strategy to fabricate a WLED is by using a blue InGaN-based chip and YAG: Ce^{3+} converter. However, the devices based on YAG:Ce^{3+} phosphor suffer the drawbacks of high correlated color temperature (CCT) and poor color rendering index (CRI<80), due to the scarcity of red component[5]. The solution to this problem is to pump red, green and blue tricolor emission phosphors utilizing a near-ultraviolet (NUV) LED to generate excellent CRI and adjustable CCT[6,7]. At present high-performance WLEDs have been obtained by combining NUV LED chip with the red phosphor $Y_2O_2S:Eu^{3+}$, the blue phosphor $BaMgAl_{10}O_{17}:Eu^{2+}$ and the green phosphor $ZnS:Cu^{+},Al^{3+}$. However, the external quantum efficiency of the red phosphor $Y_2O_2S:Eu^{3+}$ is lower than those of the green and blue phosphors[8]. Moreover, the red phosphor is chemically unstable and has a short working lifespan, owing to the releasing of sulfide gas. Therefore, it's necessary to develop novel red phosphors which represent intense emission efficiently under NUV excitation in the range of 330–430 nm. It is noted that silicate-based materials are good hosts due to their excellent chemical stability, mild synthesizing conditions and lower production cost than nitrides[9]. Therefore, silicate-based compounds, such as $Ba_3Mg_2Si_2O_8:Eu^{2+},Mn^{2+}$[10], $Sr_3Al_{10}SiO_{20}:Ce^{3+},Mn^{2+}$[11] and $Sr_2Ba(AlO_4F)_{1-x}(SiO_5)_x:Ce^{3+}$[12], have been widely studied recently. In this paper, we choose $Ba_2Gd_2Si_4O_{13}$ as the host which is a newly-found silicate compound[13].

Microwave (MW) firing technique has been advanced for the synthesis of inorganic compounds. And the pioneering research in this field is from Voss and Tinga in 1968[14]. Currently, the application of MW energy for functional materials has rapidly emerged as an innovative and feasible technology with various advantages, such as rapid synthesis, energy saving and internal heating[15-17]. Recently, many materials, such as ceramics, nano-structured metal oxides and metal-based sulphides, have been prepared by MW technique[18-20]. To the best of our knowledge, the MW firing technique applied to $Ba_2Gd_2Si_4O_{13}$ synthesis has not been clarified yet.

In this paper, we prepare $Ba_2Gd_2Si_4O_{13}:Eu^{3+}$ phosphors by MW technique and solid-state (SS) method. The structural and luminescent properties of phosphors are systemically studied. A luminescence enhancement is observed by MW technique. The heating mechanism of MW synthesis is investigated in detail. Our research may

* This work has been supported by the National Natural Science Foundation of China (Nos.51002068, 51272097 and 61265004), and the National Natural Science Foundation for Youths of Yunnan (No.2012FD009).

** E-mail: qiu@kmust.edu.cn

further extend the understanding of MW synthesis, and Eu^{3+}-activated $Ba_2Gd_2Si_4O_{13}$ provides a novel platform to design and prepare red emission phosphors for WLEDs.

High purity $BaCO_3$ (A.R.), Gd_2O_3 (99.99%), SiO_2 (99.99%) and Eu_2O_3 (99.99%) were used as the starting chemicals. In addition, for Eu^{3+}:0.05% of Gd^{3+} (BGES), the stoichiometrically weighed powder samples were synthesized by utilizing MW synthesis and SS method, respectively. The raw chemicals were first mixed uniformly in an agate mortar. Then, the properly-blended powders were heated at 1200 °C and 1300 °C by SS method for 180 min and by MW synthesis for 60 min in an MW furnace (2.45 GHz, 1.5 kW, maximum temperature of 1600 °C, HAMi-Lab-V1500, SYNOTHERM Co. Ltd, China), respectively.

The phases of the as-prepared powders were identified by X-ray diffraction (XRD) patterns with Cu Kα radiation (Rigaku D/max-2500/pc, Japan). The photoluminescence (PL) spectra were performed on a HITACHI F-4600 fluorescence spectrophotometer using xenon lamp as the excitation source. The reflection spectra were recorded by a TU-1901 plus dual beam UV-VIS spectrophotometer, which was carefully calibrated with $BaSO_4$ powders. Finally, structural identification of surface morphology was observed on a scanning electron microscope (SEM) (JEOL JSM-6700F, Japan).

Fig.1 displays the XRD patterns of as-synthesized $Ba_2Gd_2Si_4O_{13}$:Eu^{3+} powders heated at different temperatures by SS and MW synthesis methods. It is confirmed that the coexistence of $Ba_2Gd_2Si_4O_{13}$ phase with a $BaSiO_3$ phase in a small amount is observed for samples prepared at 1200 °C. With the increase of firing temperature from 1200 °C to 1300 °C, the crystallization of all samples is significantly improved and the other impurity phases are not identified. $Ba_2Gd_2Si_4O_{13}$ represents a new silicate structure with a=1.2896(3) nm, b=0.5212(1) nm, c=1.7549(4) nm, β=104.08(3)° and Z=4, which contains Gd_2O_{12} dimers and finite zigzag-shaped Si_4O_{13} chains[13]. Ba^{2+} and Gd^{3+} cations are located at the sites corresponding to the point group symmetry of C_1. Furthermore, the ionic radius of Gd^{3+} (0.0938 nm CN=6) is more similar to that of Eu^{3+} (0.0947 nm CN=6) compared with those of Si^{4+} (0.026 nm CN=4) and Ba^{2+} (0.142 nm CN=8). On the basis of effective ionic radius and charge balance, it is demonstrated that Eu^{3+} ions substitute the sites of Gd^{3+} preferably.

Fig.2 shows the schematic diagrams for formation mechanisms of SS method and MW synthesis of $Ba_2Gd_2Si_4O_3$:Eu^{3+} powders. In Fig.2(a), the surfaces of starting materials fabricated by SS method first generate a relatively high temperature. Then, a part of thermal energy transfers to inside components gradually, resulting in an asymmetrical heating process. And the aggregation of the components may occur. On the contrary, it is clearly demonstrated in Fig.2(b) that MW firing is a heating method not from surfaces but from the internal, which induces the characteristic merits of homogeneous sintering and firing in a short processing time. The microwave energy absorbed by reagents produces the thermal energy, which can be expressed by the power absorbed per unit volume as[21,22]

$$P = \sigma |E|^2 = 2\pi f \varepsilon_0 \varepsilon_{\mathrm{ef}}'' |E|^2 = 2\pi f \varepsilon_0 \varepsilon_{\mathrm{r}}' \tan\delta |E|^2, \quad (1)$$

where E is the magnitude of the internal electric field (V/cm), f is the microwave frequency, ε_0 is defined as permittivity of free space, $\varepsilon_{\mathrm{ef}}''$ is the relative effective dielectric factor, $\varepsilon_{\mathrm{r}}'$ stands for the relative dielectric constant, tanδ represents the energy loss corresponding to the capacity of assimilated energy, and σ denotes the total effective conductivity. According to Eq.(1), it is shown that the dielectric properties of ε_0, σ, $\varepsilon_{\mathrm{ef}}''$, $\varepsilon_{\mathrm{r}}'$ and tanδ all play crucial roles in the energy absorbing capability of materials. For various media, there are different $\varepsilon_{\mathrm{r}}'$ and tanδ. And the tanδ can be changed with the variation of temperature. Dielectric loss (δ) may decline in MW firing process, which indicates a temperature self-balance. In this case, materials can be heated integrally, and there is no overheating. Consequently, it is prone to generate homogeneous and ragged micro-surfaces of phosphor. However, there is lack of actual dielectric data and dielectric loss factor which can be regarded as a function of temperature, resulting in the difficulty of estimating the microwave energy exerted on the microwave-absorbed materials[19,23]. In the beginning of the experiments, the ceramics of zirconium dioxide and silicon carbide can assimilate microwave energy for heating, amd their parameters of $\varepsilon_{\mathrm{r}}'$ are estimated to be 20–30 and 10.3, respectively. With the increase of firing temperature, the increase of dielectric loss for $Ba_2Gd_2Si_4O_{13}$ may act as an important role in the MW firing process[19,24,25].

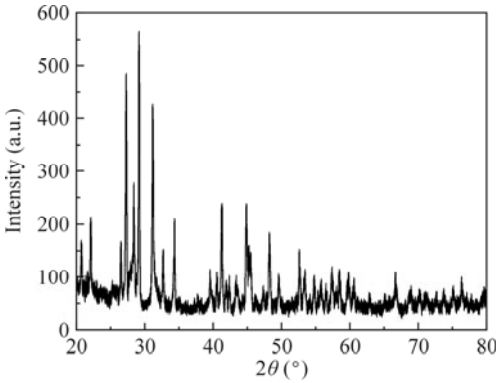

(a) 0.5% NH_4F at 1300 °C, SS

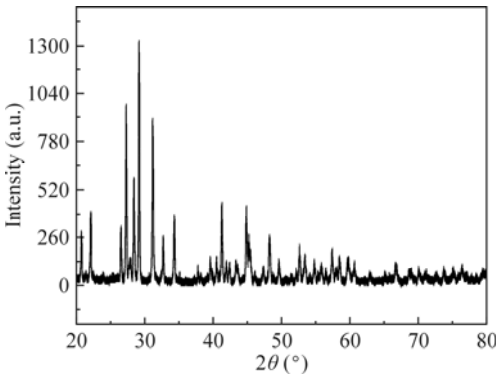

(b) 0.5% NH_4F at 1300 °C, MW

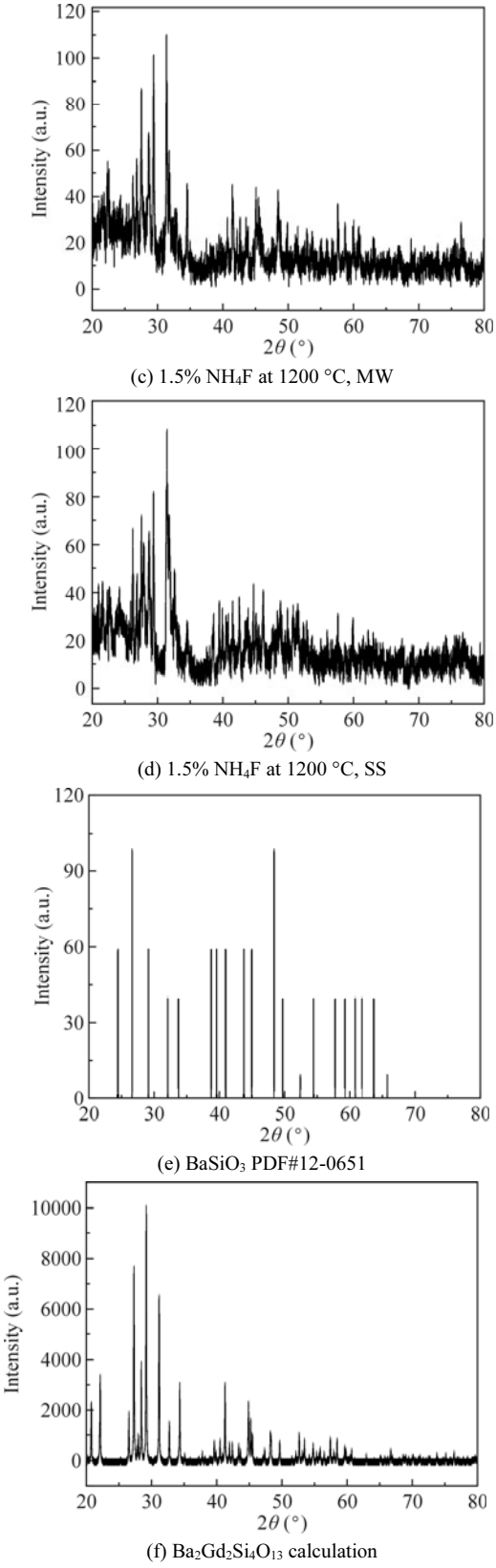

(c) 1.5% NH_4F at 1200 °C, MW

(d) 1.5% NH_4F at 1200 °C, SS

(e) $BaSiO_3$ PDF#12-0651

(f) $Ba_2Gd_2Si_4O_{13}$ calculation

Fig.1 XRD patterns of the synthesized $Ba_2Gd_2Si_4O_{13}:Eu^{3+}$ powders with varied temperatures by SS and MW firing methods

The diffuse reflection spectra of BGES prepared by SS method and MW synthesis are shown in Fig.3. In the absorption region of 200–540 nm, there are several characteristic sharp absorption bands peaked around 393 nm, 464 nm and 534 nm, which are assigned to the transitions from ground state to excited states of Eu^{3+}, i.e., $^7F_0 \rightarrow {}^5L_6$, $^7F_0 \rightarrow {}^5D_2$ and $^7F_1 \rightarrow {}^5D_1$. It is observed from Fig.3 that there is a broad absorption band centered at 255 nm originating from the valence-to-conduction transitions of $Ba_2Gd_2Si_4O_3$ matrix lattice. And there is an absorption band in the range of 200–300 nm, which can be attributed to the well-known charge transfer state (CTS) absorption transitions between the completely filled 2p orbital for O^{2-} ions and the partially filled 4f orbital for Eu^{3+} ions. Furthermore, the position of the absorption band significantly depends on the material matrix lattice. It should be noted that there is a red shift from 255 nm to 282 nm, which may be due to the micro-structures of $Ba_2Gd_2Si_4O_3:Eu^{3+}$ synthesized by MW firing can decrease the charge migration energy from the micro-locality of the host to Eu^{3+} luminescence emitters. Moreover, the absorption intensity of BGES prepared by MW synthesis from 270 nm to 400 nm is clearly stronger than that of sample synthesized by SS method. The results indicate that the absorption enhancement may promote the increase of efficient excitation energy absorbed by BGES phosphor for the ultimate luminescence.

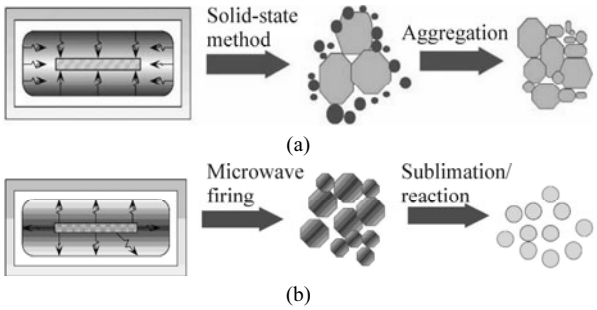

Fig.2 Formation mechanisms of (a) SS method and (b) MW synthesis for $Ba_2Gd_2Si_4O_3:Eu^{3+}$ powders

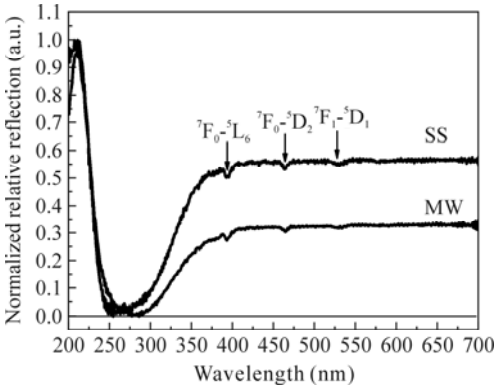

Fig.3 Normalized diffuse reflection spectra of $Ba_2Gd_2Si_4O_3:Eu^{3+}$ samples synthesized by SS method and MW synthesis at 1300 °C

In order to confirm the absorption properties, the excitation spectra of BGES monitored at 612 nm emission

($^5D_0$-$^7F_2$) are measured as shown in Fig.4. The excitation spectra contain some sharp peaks in the range of 300–550 nm, which are associated with the characteristic intra-configurational 4f-4f transitions of Eu^{3+} ions. Besides, the specific absorption bands of the $^7F_0 \rightarrow {}^5L_6$ transition at 393 nm and the $^7F_0 \rightarrow {}^5D_2$ transition at 465 nm match well with the emission wavelengths of NUV or blue LED chips, which demonstrates the potential applications in the fabrication of phosphor-converted WLED. It is noted that the enhancement of excitation spectrum (λ_{em}=612 nm) for $Ba_2Gd_2Si_4O_3$:Eu^{3+} sample sintered by MW synthesis is observed, which is consistent with the result of diffuse reflection spectra shown in Fig.3.

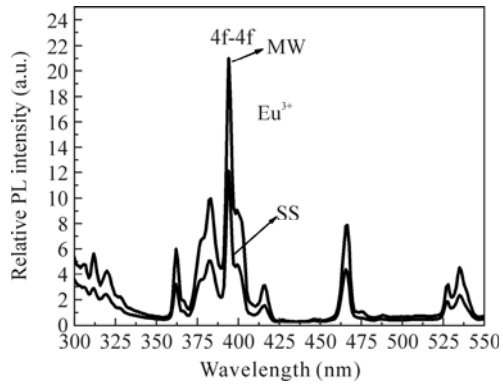

Fig.4 Excitation spectra of $Ba_2Gd_2Si_4O_3$:Eu^{3+} samples synthesized by SS method and MW synthesis with λ_{em}=612 nm

Upon 393 nm and 464 nm excitation in Eu^{3+}-activated $Ba_2GdSi_4O_{13}$ powder, the strong brightness of red PL is distinctly observed. As shown in Fig.5(a), the emission spectra consist of characteristic emission lines due to the electric transitions of Eu^{3+} ions from $^5D_0$ excited state to the ground states of ^7F_J (J=0–4) in $4f^6$ configuration[8,26]. The $^5D_0 \rightarrow {}^7F_2$ transition with ΔJ=2 of Eu^{3+} ion is hypersensitive, and the electric-dipole transition intensity can be tailored by order of magnitude depending on Eu^{3+} local environment in host lattices. The intensity of the $D_0 \rightarrow {}^7F_2$ transition decreases as the site symmetry of Eu^{3+} ion increases. In general, the PL intensity ratio of the $^5D_0 \rightarrow {}^7F_2$ transition to the $^5D_0 \rightarrow {}^7F_1$ transition can always be regarded as a sensitive probe of the site symmetry and the coordination surroundings of Eu^{3+}. As shown in Fig.5(a), the intensity ratio of the $^5D_0 \rightarrow {}^7F_2$ transition (around 600–640 nm) to $^5D_0 \rightarrow {}^7F_1$ transition (around 583–600 nm) is about 3.1 for BGES synthesized by MW firing technique under 393 nm excitation. The result implies that Eu^{3+} ions are located in asymmetric sites of cations in $Ba_2Gd_2Si_4O_{13}$ host. This is in agreement with the crystal structure of Eu^{3+} ions which substitute Gd^{3+} sites. In addition, the presence of parity forbidden $^5D_0 \rightarrow {}^7F_0$ transition around 579 nm is ascribed to the mixing of *J*-*J* levels for Eu^{3+} ions by crystal field effects, demonstrating the absence of inversion symmetry at the sites of Eu^{3+} in $Ba_2Gd_2Si_4O_{13}$ lattices. Besides, it is surprising to notice that the integrated emission intensity of Eu^{3+} in $Ba_2Gd_2Si_4O_{13}$ host lattices synthesized by MW firing-incubation is about 1.9 times stronger in the range of 560–720 nm than that of sample sintered by SS method under the excitation of 393 nm. To further understand the PL properties of Eu^{3+} ions, the luminescent color of $Ba_2Gd_2Si_4O_{13}$:Eu^{3+} powder synthesized by MW synthesis excited by 393 nm (labeled as a-393ex-MW) is characterized via Commission International de I'Eclairge (CIE) chromaticity diagram as shown in Fig.5(b). It shows that the color coordinate (x=0.65, y=0.35) is located in the reddish orange region, which demonstrates the feasible applications in solid-state lighting.

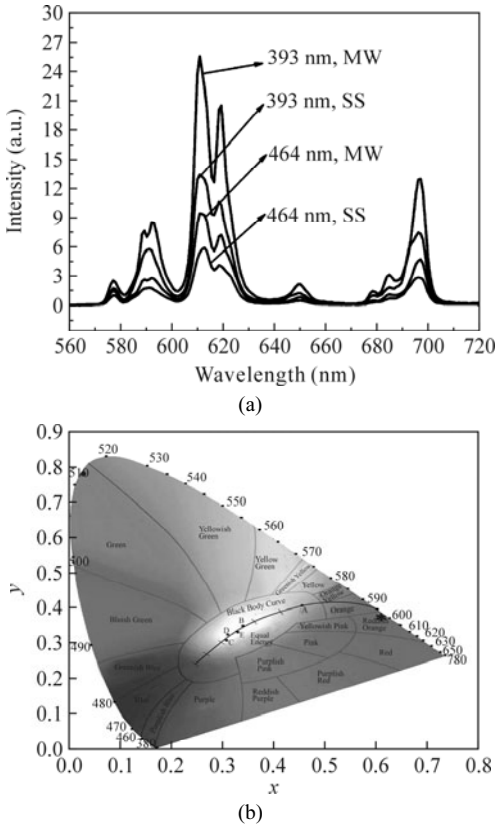

Fig.5 (a) Emission spectra of $Ba_2Gd_2Si_4O_{13}$:Eu^{3+} samples synthesized by SS and MW methods at 1300 °C under λ_{ex}=393 nm and 464 nm; (b) CIE chromaticity diagram related to the sample prepared by MW firing process under 393 nm excitation

In order to further understand the mechanism of PL enhancement, the SEM images of BGES powders prepared by SS and MW synthesis methods are measured. As shown in Fig.6(a), concave-convex surfaces and fine uniformity of about 2 μm size grains of the synthesized sample are achieved, which exhibit excellent effects for fluorescence intensity and emission lifetime. In addition, as shown in Fig.6(b), the grain-based agglomeration phenomenon of the sample prepared by SS method is observed. And the agglomeration of phosphor particles may induce a bad effect on the luminescent properties of BGES due to poor absorption and scattering of the excitation light.

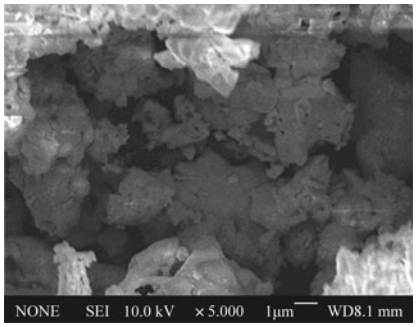

(a)

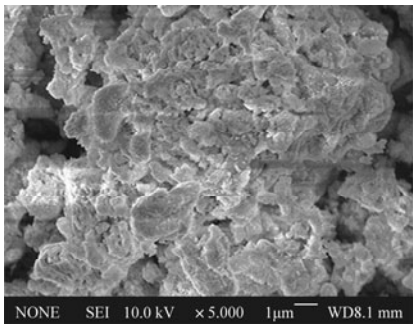

(b)

Fig.6 SEM photographs of $Ba_2Gd_2Si_4O_3:Eu^{3+}$ samples synthesized by (a) MW and (b) SS methods

In conclusion, a series of novel $Ba_2Gd_2Si_4O_{13}:Eu^{3+}$ phosphors are successfully fabricated by SS method and an economical feasible and rapid MW technique for the first time. The obtained phosphors exhibit characteristic red fluorescence which can be ascribed to the electric transitions $^5D_0 \rightarrow {}^4F_J$ (J=0–4) of Eu^{3+} ions. The integrated emission intensity of $Ba_2Gd_2Si_4O_{13}:Eu^{3+}$ prepared by MW firing synthesis is about 1.9 times stronger than that of sample fabricated by SS method excited at 393 nm. The mechanism of the MW firing-incubation process is investigated. SEM images indicate that the formed concave-convex surfaces and uniform grains synthesized by MW firing can demonstrate good effects on fluorescence intensity and emission lifetime. Our research may further promote the understanding of MW synthesis, and the results indicate that $Ba_2Gd_2Si_4O_{13}:Eu^{3+}$ is a promising red emitting phosphor applied in solid-state lighting and display field.

References

[1] Lee G. Y., Im W. B., Kirakosyan A., Cheong S. H., Han J. Y. and Jeon D. Y., Optics Express **21**, 3287 (2013).

[2] Yang Zhang, Guogang Li, Dongling Geng, Mengmeng Shang, Chong Peng and Jun Lin, Inorganic Chemistry **51**, 11655 (2012).

[3] Hong Yu, Wenwen Zi, Shi Lan, Shucai Gan, Haifeng Zou, Xuechun Xu and Guangyan Hong, Optics and Laser Technology **44**, 2306 (2012).

[4] LI Jian, DENG Jia-chun, LU Qi-fei and WANG Da-jian, Optoelectronics Letters **9**, 293 (2013).

[5] Yang P., Yu X., Yu H., Jiang T., Xu X., Yang Z., Zhou D., Song Z., Yang Y., Zhao Z. and Qiu J., Journal of Luminescence **135**, 206 (2013).

[6] PANG Li-bin, GAO Shao-jie, GAO Zhan-jun, LI Hong-lian and WANG Zhi-jun, Optoelectronics Letters **9**, 282 (2013).

[7] MAO Zhi-yong, WANG Da-jian, LIU Yan-hua, FEI Qin-ni, ZHENG Xi, XU Suo-cheng and QIU Kun, Optoelectronics Letters **6**, 116 (2010).

[8] Yu R., Noh H. M., Moon B. K., Choi B. C., Jeong J. H., Jang K., Yi S. S. and Jang J. K., Journal of Alloys and Compounds **576**, 236 (2013).

[9] Xiao-Ming Wang, Chun-Hai Wang, Xiao-Jun Kuang, Ru-Qiang Zou, Ying-Xia Wang and Xi-Ping Jing, Inorganic Chemistry **51**, 3540 (2012).

[10] Ma L., Wang D. J., Mao Z. Y., Lu Q. F. and Yuan Z. H., Applied Physics Letters **93**, 144101 (2008).

[11] Nag A. and Kutty T. R. N., Materials Chemistry and Physics **91**, 524 (2005).

[12] Denault K. A., George N. C., Paden S. R., Brinkley S., Mikhailovsky A. A., Neuefeind J., DenBaars S. P. and Seshadri R., Journal of Materials Chemistry **22**, 18204 (2012).

[13] Wierzbicka-Wieczorek M., Kolitsch U. and Tillmanns E., Acta Crystallographica Section C-Crystal Structure Communications **66**, I29 (2010).

[14] Ishigaki T., Mizushina H., Uematsu K., Matsushita N., Yoshimura M., Toda K. and Sato M., Materials Science and Engineering: B **173**, 109 (2010).

[15] Uematsu K., Toda K. and Sato M., Journal of Alloys and Compdunds **389**, 209 (2005).

[16] Jung K. Y. and Kang Y. C., Physica B **405**, 1615 (2010).

[17] Cao L. S., Lu Q. F., Wang L. C., Li J., Song J. and Wang D. J., Ceramics International **39**, 7717 (2013).

[18] Agrawal D. K., Current Opinion in Solid State Materials Science **3**, 480 (1998).

[19] Bilecka I. and Niederberger M., Nanoscale **2**, 1358 (2010).

[20] Tang Y. X., Guo H. P. and Qin Q. Z., Solid State Communications **121**, 351 (2002).

[21] Ishigaki T., Mizushina H., Uematsu K., Matsushita N., Yoshimura M., Toda K. and Sato M., Materials Sciences & Engineering. B, Solid-State Materials for Advanced Technology **173**, 109 (2010).

[22] Rao K. J., Ramakrishnan P. A. and Gadagkar R., Journal of Solid State Chemistry **148**, 100 (1999).

[23] Shukla A. K., Mondal A. and Upadhyaya A., Science of Sintering **42**, 99 (2010).

[24] Leveque J. M. and Cravotto G., Chimia International Journal for Chemistry **60**, 313 (2006).

[25] Das S., Mukhopadhyay A. K., Datta S. and Basu D., Bulletin Materials Science **31**, 943 (2008).

[26] QIU Kun, XU Suo-cheng, TIAN Hua, ZHENG Xi, LV Tian-shuai, LU Qi-fei and WANG Da-jian, Optoelectronics Letters **7**, 350 (2011).